Chinese Chemical Letters 37 (2026) 112696

Contents lists available at ScienceDirect

Chinese Chemical Letters

journal homepage: www.elsevier.com/locate/cclet

# Recent advances in annihilator design and assembly for triplet-triplet annihilation upconversion

Junjie Wen, Dantong Chen, Hongli Cao, Xue Li, Ying Qin, Cheng Yang*, Wanhua Wu*

*Key Laboratory of Green Chemistry & Technology, College of Chemistry, Sichuan University, Chengdu 610064, China*

ARTICLE INFO

*Article history:*
Received 26 November 2025
Revised 20 March 2026
Accepted 30 March 2026
Available online 31 March 2026

*Keywords:*
Upconversion
Annihilators
Multichromophoric
Macrocyclic
Orderly arranging

ABSTRACT

Triplet-triplet annihilation upconversion (TTA-UC), a process capable of converting low-energy photons into higher-energy light, has garnered significant interest for applications in photovoltaics, bioimaging, and photopolymerization. This phenomenon relies on the concerted interaction between a sensitizer (energy donor) and an annihilator (energy acceptor). While considerable research has been devoted to developing diverse molecular derivatives of photosensitizers with tailored photophysical properties, the deliberate structural design of annihilators has remained relatively underexplored. However, in molecular diffusion-limited systems, such as in solid-state matrices, rational annihilator design becomes crucial. This review summarizes recent advances in the structural design of triplet annihilators for TTA-UC systems. We categorize these emerging annihilators into three groups based on their design principles: (1) Multichromophoric annihilators engineered for intramolecular TTA, (2) supramolecular macrocycle-based annihilators that enhance both triplet-triplet energy transfer and TTA processes, and (3) annihilators designed with ordered molecular arrangements to achieve efficient TTA-UC in diffusion-limited environments.

© 2026 Published by Elsevier B.V. on behalf of Chinese Chemical Society and Institute of Materia Medica, Chinese Academy of Medical Sciences.

Upconversion (UC), an anti-Stokes process that converts low-energy photons into high-energy emission, has attracted considerable research interest due to its potential for improving the overall efficiency of solar energy utilization [1–5]. Among various upconversion techniques, such as those employing two-photon absorption dyes [6,7], or rare earth metal materials [8–13], triplet–triplet annihilation-based upconversion (TTA-UC) stands out for its unique advantages [14–19]. These include the ability to be excited by low-power incoherent light (even under terrestrial solar radiation) [20–23], high upconversion quantum efficiency, and tunable excitation/emission wavelengths through appropriate selection of sensitizers and annihilators. These merits make TTA-UC highly promising for a range of cutting-edge applications, including photocatalysis [24–27], bioimaging [28–30], 3D printing [31,32], and photodynamic therapy [33–37].

In a typical TTA-UC process, the sensitizer (energy donor) and annihilator (energy acceptor) work in concert to achieve photon upconversion. The sensitizer first absorbs low-energy photons, populating its singlet excited state, which then undergoes intersystem crossing (ISC) to generate a triplet excited state. Subsequently, triplet–triplet energy transfer (TTET) from the sensitizer to the annihilator populates the triplet state of the latter. When two such triplet annihilators encounter each other, they can undergo triplet–triplet annihilation (TTA), resulting in the formation of a singlet excited state at a higher energy. Radiative decay from this singlet state produces delayed fluorescence, *i.e.*, upconverted emissions. A schematic illustration of this photophysical mechanism is provided in Fig. 1.

In TTA-UC systems, the critical steps of TTET and TTA operate *via* the Dexter energy transfer mechanism [38–42]. A fundamental requirement for this process is the diffusion-assisted close encounter of the species involved within their triplet excited-state lifetimes. Consequently, a central research direction for improving TTA-UC efficiency has been to extend the triplet lifetimes of molecular components [41,43]. To this end, numerous photosensitizers with tailored photophysical properties have been synthesized, including Pt–Pd(II) porphyrin complexes, Ru(II), Pt(II), Ir(III), Re(I), Fe(III), and Cu(I) based metal complexes [44–55], as well as organic triplet sensitizers [56–60], among others [61–64]. These developments have markedly enhanced TTET efficiencies, leading to upconversion quantum yields of up to 20% in solutions [39,43].

On the other hand, the annihilator, as another essential component in TTA-UC systems, plays a critical role in determining the overall upconversion efficiency. An ideal annihilator should satisfy four key design criteria: (1) A triplet excited state lower in energy than that of the sensitizer; (2) a singlet state lying below twice

* Corresponding authors.
*E-mail addresses:* yangchengyc@scu.edu.cn (C. Yang), wuwanhua@scu.edu.cn (W. Wu).

https://doi.org/10.1016/j.cclet.2026.112696
1001-8417/© 2026 Published by Elsevier B.V. on behalf of Chinese Chemical Society and Institute of Materia Medica, Chinese Academy of Medical Sciences.

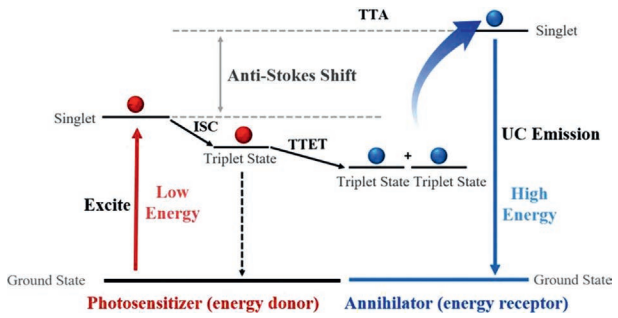



**Fig. 1.** The schematic diagram illustrating the mechanism and energy transfer process of TTA-UC. The red ball represents the excitons of the sensitizer, and the blue ball represents the excitons of the annihilator.

the energy of its triplet state to render TTA energetically feasible; (3) a high fluorescence quantum yield ($\Phi_{FL}$); and (4) inaccessibility of the $T_2$ state following the TTA process. These requirements are readily met in many acene derivatives, such as diphenylanthracene (DPA) [65–67], rubrene [68,69], and perylene [70]. As a result, such commercially available parent molecules have been widely adopted as annihilators, with relatively limited efforts devoted to deliberating molecular structural design. One contributing reason was that the triplet lifetime of annihilators typically far exceeds that of metal complexes, making the TTA process in solution largely diffusion-controlled.

More recently, growing interest has been directed toward solid-state TTA-UC, motivated by its practical benefits in processing and device integration [71–73]. However, achieving high-efficiency TTA-UC in solid matrices remains challenging. Many efforts have been made to exploit new matrices or new strategies for efficient solid-state TTA-UC. Significant strides have been made since the first report on solvent-free solid-state systems in 2007 [17], but UC efficiency hitherto obtained at solid state is far from satisfying. In most cases, the UC quantum yield was <5% (out of a 50% maximum) [74–76]. A major limiting factor is the restricted molecular diffusion in solids, which hinders exciton migration and suppresses both TTET and TTA, resulting in weak upconversion emission [77,78]. Although high concentrations of both sensitizer and annihilator are commonly used to improve energy transfer and encounter probability, this often leads to uncontrolled aggregation of the sensitizer and annihilator due to poor miscibility in solid hosts. To assure efficient TTA-UC in solid-state, besides the aforementioned criteria for the annihilators, the following critical aspects should also be considered when designing and assembling annihilators: (1) The precisely engineered interchromophoric distance (both between sensitizer and annihilator and between annihilators themselves) to ensure molecular orbital overlap in diffusion-limited environment; (2) an optimized orientation of the chromophores to assure a larger spin statistics factor *f* during the TTA process; and (3) an order arrangement of the annihilators to assure fast triplet exciton migration.

Focusing on the requirements for annihilators in solid-state upconversion, this review systematically summarizes recent advances in annihilator design and assembly strategies for enhanced TTA-UC. The discussed annihilators are strategically categorized into three groups based on their design motifs: (1) Multichromophoric annihilators engineered for intramolecular TTA, (2) supramolecular macrocycle-based annihilators to enhance both TTET and TTA processes, and (3) annihilators with ordered molecular arrangements to achieve efficient TTA-UC in diffusion-limited environments. It should be noted that this review emphasizes structural derivatization and strategic assembly. Therefore, many commercially available acene compounds that are employed as annihilators to achieve upconverted emission at various wavelengths are not covered here [79–82].

## 1. Multichromophoric annihilators for intramolecular TTA

The upconversion quantum yield ($\Phi_{UC}$) is a key parameter for evaluating the overall performance of a triplet–triplet annihilation upconversion (TTA-UC) system. It is defined as the ratio of emitted upconverted photons to incident photons absorbed by the sensitizer and can be expressed as the product of the quantum yields of each elementary step involved:

$$\Phi_{UC} = 1/2 \times f \times \Phi_{ISC} \times \Phi_{TTET} \times \Phi_{TTA} \times \Phi_{F} \quad (1)$$

here, $\Phi_{ISC}$, $\Phi_{TTET}$, $\Phi_{TTA}$, and $\Phi_{F}$ represent the quantum yields of intersystem crossing of the sensitizer, triplet–triplet energy transfer from the sensitizer to the annihilator, triplet–triplet annihilation between two annihilators, and the fluorescence of the annihilator, respectively. The factor *f* denotes the probability of forming a singlet state *via* TTA. The prefactor 1/2 reflects that two triplet states are consumed to produce one upconverted photon, thereby setting the theoretical maximum efficiency of TTA-UC at 50%.

The UC intensity typically exhibits a quadratic dependence on incident light intensity at low power densities, transitioning to a linear regime under high-power excitation, where the quantum yield reaches its maximum. This transition point is defined as the threshold intensity ($I_{th}$). $I_{th}$ is another critical performance parameter for TTA-UC, and achieving a low $I_{th}$ is essential for enhancing the utilization efficiency of low-intensity light sources such as sunlight. Several factors influence $I_{th}$, including the concentrations of the sensitizer and annihilator, the diffusion coefficient of triplet excitons in the medium, the triplet lifetime of the annihilator ($\tau_T$), and the triplet–triplet annihilation rate constant ($k_{TTA}$). In general, low $I_{th}$ is more readily attained in solution-based systems due to efficient molecular diffusion. In contrast, solid-state systems often exhibit significantly higher $I_{th}$ as a result of restricted molecular motion. Therefore, optimizing the molecular structure of annihilators to extend $\tau_T$ and enhance $k_{TTA}$ represents effective strategies for reducing $I_{th}$ and improving TTA-UC performance.

In response to a high $\Phi_{UC}$ and low $I_{th}$, various TTA-UC systems operating *via* "intramolecular TTA" have been developed. These systems consist of two or more annihilator units linked through either conjugated [83–85] or non-conjugated [86–89] bridges. This design strategy covalently integrates the annihilating units within a single molecular framework, thereby converting a stochastic, diffusion-dependent intermolecular process into a directed, intramolecular one. The key to this approach lies in precisely tuning the spatial separation and relative orientation of the annihilating moieties. These factors directly modulate the bimolecular rate constant of TTA ($k_{TTA}$) and the spin statistics factor *f*. Optimizing these parameters is crucial, as they significantly influence both the quantum yield of TTA-UC and the threshold intensity ($I_{th}$).

Covalently tethering DPA annihilators to a polymeric backbone has been reported (compounds **A-2** and **A-3**, Fig. 2) [90,91], **A-1** was an unpolymerized monomer. A broad range of annihilator contents, ranging from 8 wt% to 72 wt%, could be incorporated into the glassy upconverting materials without phase separation. When physically mixed with 0.05 wt% **S-1** as the sensitizer, these films exhibited green-to-blue (543 nm to 440 nm) upconversion at power densities as low as 32 mW/cm$^2$ [90]. However, these TTA-UC systems showed very limited quantum yields, partly due to inefficient intermolecular TTET process from the sensitizer to the annihilators [91].

To address this limitation, photoactive polymers consisting of a ruthenium tris(bipyridyl) complex ($Ru(bpy)_3$) core and pendant DPA arms (compounds **A-4** and **A-5**) were developed [92,93]. Efficient intramolecular triplet energy transfer from the photoexcited

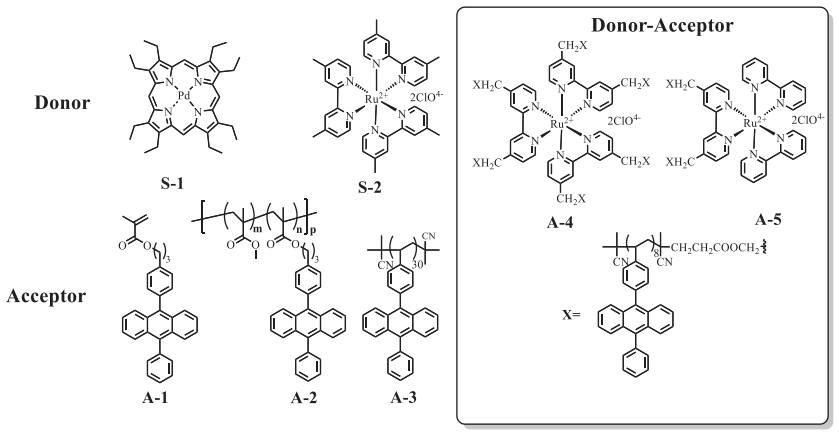



**Fig. 2.** Chemical structures of the sensitizer **S-1** and **S-2**, the annihilators of unpolymerized monomer **A-1**, and polymers **A-2**∼**A-5**.

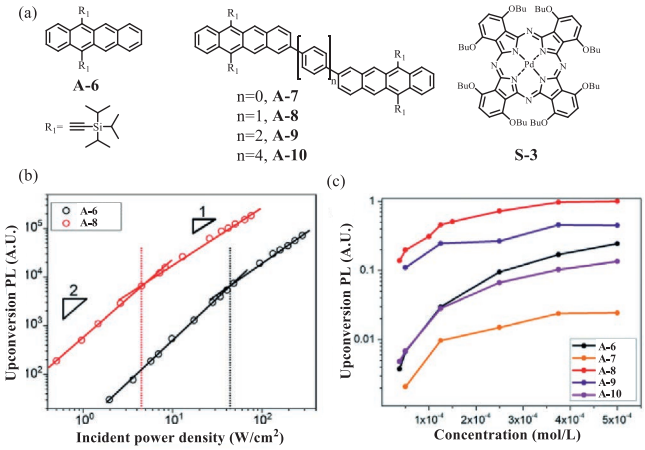



**Fig. 3.** (a) Structures of the compounds **A-6**∼**A-10** and **S-3**. (b) Dependence of upconverted PL on incident light intensity at $2.5 \times 10^{-4}$ mol/L **A-6** and **A-8** concentration. The transition between quadratic and linear dependences occurs at 44.5 and 4.3 W/cm$^2$ for **A-6** and **A-8.** Reproduced with permission [94]. Copyright 2019, Royal Society of Chemistry. (c) Change in upconversion PL of compounds studied as a function of annihilator concentration at $2.5 \times 10^{-5}$ mol/L **S-3**. Reproduced with permission [94]. Copyright 2019, Royal Society of Chemistry.

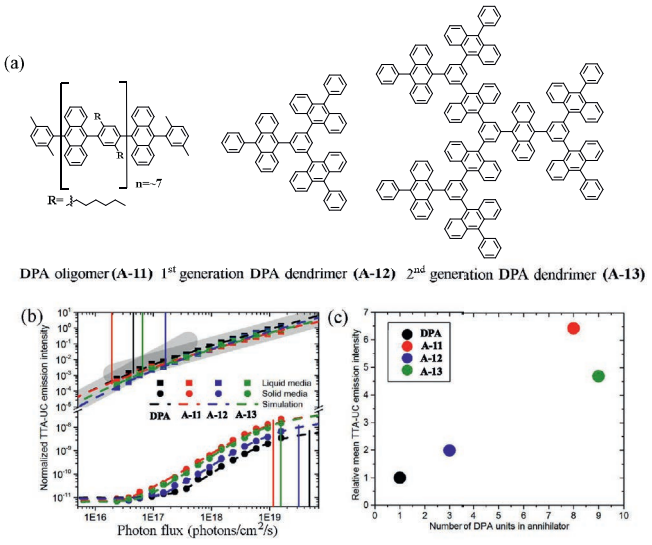



**Fig. 4.** (a) Chemical structures of DPA oligomer (**A-11**), first-generation DPA dendrimer (**A-12**), and second-generation DPA dendrimer (**A-13**). (b) Steady-state UC emission power ramp experiment with DPA, **A-11**∼**A-13** dissolved in toluene ("liquid") and in PMMA ("solid"). (c) Mean of the relative TTA-UC emission in solid media in the excitation intensities range between $3.7 \times 10^{17}$ and $1.6 \times 10^{18}$ photons cm$^{-2}$ s$^{-1}$. Reproduced with permission [86]. Copyright 2016, American Chemical Society.

$Ru(bpy)_3$ core to the DPA annihilators on the macromolecular arms was observed. Owing to the long triplet lifetime of the $Ru(bpy)_3$ unit and the tailored polymer architecture, the forward triplet energy transfer from the $Ru(bpy)_3$ unit to the DPA chromophores was found to be more efficient than the singlet back-transfer following TTA, thus, significantly TTA-UC emission was observed. Nevertheless, as only one absorbing core was incorporated per polymer chain, the TTA process primarily arose from diffusional intermolecular encounters between DPA units on different chains. As a result, only a modest yield of upconverted blue fluorescence from DPA was achieved [93].

More recently, Congreve *et al.* [94] synthesized a series of novel tetracene dimers as annihilators by covalently linking two upconverting chromophores. This molecular design establishes a concentrated local microenvironment, effectively shifting the diffusion-limited intermolecular TTA process to a more efficient intramolecular pathway (Fig. 3a). Compelling evidence for this change was provided by the significantly decreased upconversion threshold ($I_{th}$). The $I_{th}$ of the dimer system (**A-8**/**S-3**) was 4.3 W/cm$^2$, more than one order of magnitude lower than that of conventional single-molecule system (44.5 W/cm$^2$ for **A-6**/**S-3**) (Fig. 3b). The UC quantum yield of the dimers was also markedly higher than the monomers, *e.g.*, 4.2 % for **A-8**/**S-3** system *vs.* 0.70 % for **A-6**/**S-3**. Moreover, the upconverted emission intensity showed an almost ideal plateau-like stability over a broad concentration range, in sharp contrast to the "normal distribution-type" profile typical of conventional systems (Fig. 3c), demonstrating that at low concentrations, the dimeric molecules had the ability to hold two triplets, which led to an intramolecular TTA process.

Albinsson *et al.* synthesized structurally rigid annihilators by covalently linking DPA monomers into a linear oligomer and two generations of dendrimers [86]. The oligomer contained an average of eight phenylanthracene subunits, while the first-generation (**A-12**) dendrimer comprised three DPA units connected through a central phenyl ring, and the second-generation (**A-13**) dendrimer consisted of nine DPA units (Fig. 4a). In toluene solution, when Pd(II) octaethylporphyrin (**S-1**) was the sensitizer, the DPA monomer exhibited the highest upconversion efficiency due to the rapid diffusion. However, this trend reversed in solid-state PMMA films, the **A-13** and **A-11**, the largest structures, showed the strongest upconversion emission, followed by **A-12**, while the

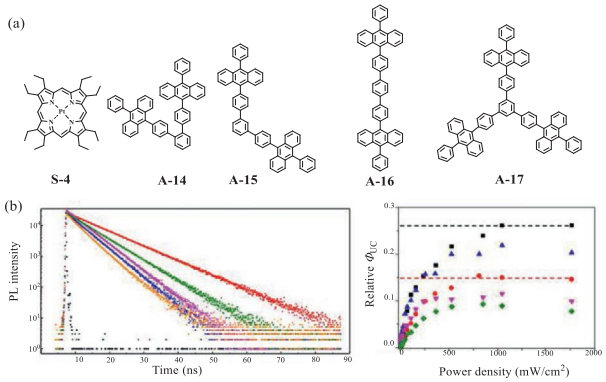



**Fig. 5.** (a) Chemical structures of DPA derivatives (**A-14**∼**A-17**). (b) Photoluminescence decays at 425 nm of the THF solution of DPA (red), **A-14** (pink), **A-15** (green), **A-16** (orange) and **A-17** (blue) under pulsed excitation at 390 nm (left) and TTA-UC quantum yield (right) as a function of excitation power density at 532 nm in solution. DPA (■), **A-14** (red ●), **A-15** (blue ▲), **A-16** (pink ▼), **A-17** (green ♦). Reproduced with permission from ref [95]. Copyright 2021 American Chemical Society.

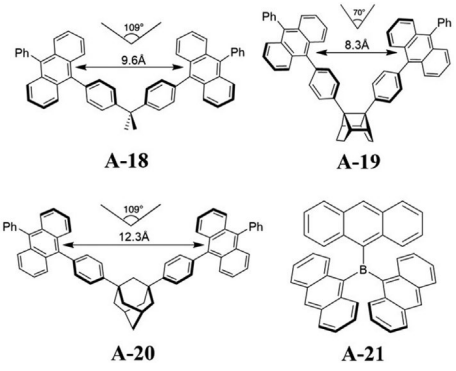



**Fig. 6.** Chemical structures of annihilators **A-18**∼**A-21**.

DPA monomer was the least efficient (Figs. 4b and c). This contrast clearly delineates the distinct dominant mechanisms in different phases: In solution, efficiency is governed by diffusion rates, favoring small, mobile molecules; whereas in solids, where molecular diffusion is severely restricted, intramolecular triplet–triplet annihilation becomes decisive. Consequently, in solid-state or highly viscous environments, extending the covalently linked molecular architecture to establish efficient intramolecular exciton migration pathways emerges as a key design strategy for achieving effective TTA-UC.

The influence of molecular geometry on the intramolecular triplet–triplet annihilation (TTA) process was further explored [95]. A series of compounds (**A-14**∼**A-17**) comprising multiple diphenylanthracene (DPA) subunits linked *via* a central benzene core was synthesized (Fig. 5a). All of these compounds exhibited satisfactory fluorescence quantum yields, comparable to that of the DPA monomer, highlighting their potential as candidate annihilators. Interestingly, the TTA-UC performance varied considerably among them. The *meta*-substituted dimer **A-15** showed the highest UC quantum yield of 21 % when paired with the sensitizer **S-4** (Fig. 5b). **A-15** showed a longer triplet lifetime, five times that of **A-16**, and therefore showed the largest statistical probability factor, which should be responsible for the efficient TTA process. Nevertheless, it is noteworthy that the TTA-UC efficiencies of these di- and trimers were all lower than that of the benchmark DPA/**S-4** system, indicating that multichromophoric emitters do not necessarily outperform single chromophores. A plausible explanation is that in a single chromophore system, many collisions that lack the required singlet character to populate the $S_1$ state result in dissociation back into free triplets, which can subsequently undergo successful triplet fusion. In contrast, for dimer or trimer systems forming multiexcitonic states, dissociation requires an additional collision. However, prior to such an event, non-radiative decay processes may lead to the deactivation of the excited states.

Ikeda *et al.* [96] also showed the important effect of the triplet lifetime of the annihilator on the TTA process. Three dyads with the DPA moieties connected by nonconjugated C1 (**A-18**), C2 (**A-19**), and C3 (**A-20**) linkages were synthesized (Fig. 6). In these dyads, the DPA units have different distances and relative orientations. It was found that the nonconjugated linkers in these systems effectively elongate the triplet lifetimes of the annihilators by suppressing nonradiative deactivation, through "intramolecular energy hopping". The triplet lifetime of **A-18**∼**A-20** was determined to be 291 ms, 249 ms and 224 ms, respectively, significantly longer than that of DPA (179 ms). However, the longer lifetime does not guarantee a larger bimolecular rate constant of TTA ($k_{TTA}$). For the three compounds, **A-19** showed the largest $k_{TTA,}$ probably due to the nearest distance and proper orientation between two DPA moieties, and correspondingly lead to a relatively lower $I_{th}$ value, which was even lower than that of DPA, while the other dyads all showed smaller $k_{TTA}$ and larger $I_{th}$ when compared with that of DPA monomer.

Enlarging the $k_{TTA}$ by structure optimization was further reported. Kobori *et al.* synthesized a TTA annihilator (**A-21**) by connecting three anthracene units in a rotationally symmetric arrangement around a boron center [88]. After populating triplet excitons in the vibronic trimer *via* energy transfer from the sensitizer PtOEP (**S-4**), rapid intramolecular migration of the excitons, also referred to as intramolecular triplet exciton hopping, was anticipated. This process substantially extended the effective collision distance between excitons through *pseudo*-rotational motion. As a result, although the triplet lifetime of **A-21** was considerably shorter than that of DPA (46.2 μs *vs.* 1.67 ms), the TTA reactivity was enhanced, leading to an increase in the $k_{TTA}$ to $1.95 \times 10^9$ L mol$^{-1}$ s$^{-1}$, compared to $1.64 \times 10^9$ L mol$^{-1}$ s$^{-1}$ in the conventional TTA-UC system using DPA.

Except DPA, perylene is another excellent annihilator in TTA-UC due to its optimal emission efficiency ($\Phi_F = 0.95$) and quite high $T_2$ state compared with the $T_1$ state. However, due to the structural planarity, perylene suffers from fluorescence quenching and excimer formation at high concentrations, and therefore, the quantum yield achieved by this annihilator was often limited. To address this problem, Duan *et al.* [97] designed an annihilator **A-22** (Fig. 7a), with two perylene chromophores connected with a flexible spacer paracyclophane, the average distance between the perylene branches was estimated to be 9.2 Å, which is large enough to avoid detrimental intermolecular interactions *via* $\pi-\pi$ stacking at high concentrations. This twisted conformation not only suppresses $\pi-\pi$ stacking but also significantly enlarges the Stokes shift. As a result, the fluorescence quantum yield ($\Phi_F$) remains nearly unchanged until the concentration exceeds $10^{-4}$ mol/L (Fig. 7b), in sharp contrast to the parent perylene compound. The emission profile of **A-22** also shows no alteration at high concentrations (Fig. 7b inset), indicating that reabsorption is effectively minimized due to the increased Stokes shift. Benefit from these excellent photophysical properties, **A-22** achieved a record red-to-green external upconversion yield of 42 %, approaching the theoretical limit of 50 % (Fig. 7c). This high efficiency corresponds to a statistical factor $f \approx 1$, indicating that not only quintet states but also higher-energy triplet pathways (*e.g.*, $T_2$) remain inaccessible during triplet-triplet annihilation. When **A-22** concentration is reduced to $10^{-4}$ mol/L, the gain in fluorescence quantum yield is counterbalanced by a loss in energy transfer efficiency, while further alter-

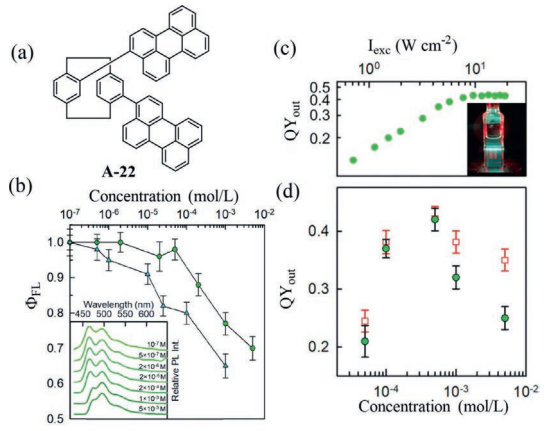



**Fig. 7.** (a) The chemical structure of **A-22**. (b) The photoluminescence quantum yield $\Phi_F$ of **A-22** (dots) and perylene (triangles) as a function of the dye concentration, inset is the photoluminescence spectra of the **A-22** solution. (c) The UC quantum yield as a function of the incident excitation intensity, inset is a digital picture of the sample and (d) comparison of theoretical $\Phi_{UC}$ values (squares) calculated using Eq. 1 from independently determined parameters *vs.* the experimental efficiency values (dots) measured as a function of **A-22** concentration. Reproduced with permission [97]. Copyright 2021, Royal Society of Chemistry.

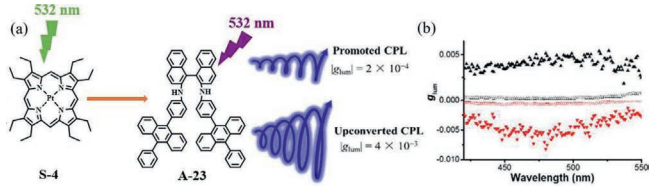



**Fig. 8.** (a) Schematic representation of CPL emission. Promoted CPL from **A-23** excited at 360 nm with $|g_{lum}| = 2 \times 10^{-4}$ and upconverted CPL from **A-23**/**S-4** mixture excited by 532 nm with $|g_{lum}| = 4 \times 10^{-3}$. (b) UC–CPL dissymmetry factor $g_{lum}$ *versus* wavelength. ▲: (*S*)-**A-23**/**S-4** excited by 532 nm laser; △: (*S*)-**A-23** excited by 360 nm laser; ▼: (*R*)-**A-23**/**S-4** excited by 532 nm laser; ▽: (*R*)-**A-23**/**S-4** excited by 360 nm laser. Reproduced with permission [98]. Copyright 2017, American Chemical Society.

ing the concentration below $10^{-4}$ mol/L or above $10^{-3}$ mol/L, a pronounced decline in $\Phi_{UC}$ was observed (Fig. 7d), mostly due to the competitive back-energy transfer from the **A-22** triplets to sensitizers.

Integrating TTA-UC with molecular chirality offers a novel route for developing advanced chiral luminescent materials, Liu, Duan, and co-workers [98] designed a chiral annihilator (**A-23**) by linking two DPA units to a binaphthyldiamine scaffold. Using **S-4** as the photosensitizer, a high upconversion quantum yield of about 11 % was achieved, highlighting excellent photon upconversion performance. Notably, upconverted circularly polarized luminescence (UC–CPL) was observed for the first time, with the luminescence chirality strictly matching the absolute molecular configuration (*R* or *S*) of the annihilator (Fig. 8a). Importantly, a synergistic enhancement of the luminescence asymmetry factor ($g_{lum}$) through multi-step photophysical processes, including triplet-triplet energy transfer (TTET) and TTA was demonstrated. For example, when chirally pure (*R*)-**A-23** or (*S*)-**A-23** solutions were directly excited at 360 nm (Xe lamp or laser) to generate down-converted emission, the $|g_{lum}|$ value was only $2 \times 10^{-4}$. In contrast, upon sensitized upconversion using a 532 nm laser in a mixture of **A-23** and **S-4**, the $g_{lum}$ value for UC–CPL increased to $4 \times 10^{-3}$, which was a 20-fold enhancement (Fig. 8b). The integration of TTA-UC with CPL opens a promising avenue for developing advanced chiral functional materials, although the precise mechanisms governing the observed amplification effects require further investigation.

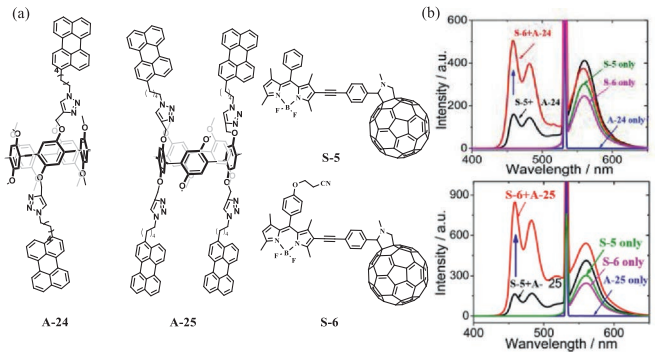



**Fig. 9.** (a) Chemical structures of supramolecular annihilators **A-24**, **A-25**, and the sensitizers **S-5** and **S-6**. (b) TTA-UC emission of **A-24** (up) and **A-25** (down) with **S-5** and **S-6** as the triplet photosensitizers, respectively. Reproduced with permission [109]. Copyright 2016, American Chemical Society.

## 2. Supramolecular macrocycle-based annihilators to enhance both TTET and TTA processes

Significant progress in optimizing TTA-UC performance has been realized through the chemical tuning of photosensitizers and annihilators [83,95,99–101]. However, further improvements are hindered not only by complex syntheses and unpredictable photophysical behaviors but also by a more fundamental constraint, the Dexter-type energy transfer mechanism itself. This process requires direct orbital overlap, limiting effective interaction to a short range (typically $< 1$ nm) [102–105]. To overcome this spatial limitation, supramolecular strategies have been developed to pre-organize sensitizer-annihilator pairs in close proximity. By utilizing noncovalent interactions, such as $\pi$-$\pi$ stacking, electrostatic attraction, and hydrogen-bonding, these approaches enable precise molecular arrangement in solution, thereby enhancing the efficiency of triplet energy transfer [106–108].

In 2016, Yang and Wu *et al.* [109] pioneered the first host-guest-based supramolecular TTA-UC system. Multiple perylene units (employed as annihilators) were grafted on a macrocyclic compound, pillar[5]arene, to achieve novel supramolecular annihilators **A-24** and **A-25** (Fig. 9a). Moreover, an alkyl nitrile chain, known to strongly bind with pillar[5]arene was attached to a $C_{60}$−BODIPY dyad, which served as a sensitizer (**S-6**). The perylene-tethered pillar[5]arenes formed stable 1:1 complex with a nitrile-bearing $C_{60}$−BODIPY dyad, showing association constants ($K_a$) of $3.7 \times 10^4$ (**S-6**/**A-24**) and $4.0 \times 10^4$ L/mol (**S-6**/**A-25**), respectively. It was found that the presence of the nitrile side chain in **S-6** hardly influenced the photophysical properties such as energy levels of both singlet and triplet states and the triplet lifetimes of the sensitizers. However, through host−guest complexation, the TTET process was significantly facilitated as the sensitizer and annihilators were positioned in close proximity, moreover, as two or four perylene units were attached to a host, the local concentration of the annihilators increased, which led to more efficient TTA processes. As such, at the diluted concentration of [sensitizer] $= 1 \times 10^{-5}$ mol/L and [annihilator] $= 3 \times 10^{-5}$ mol/L, the UC intensity of **A-24** is about 2.8-fold greater when **S-6** as the sensitizer than when **S-5** was the sensitizer. A more apparent enhancement as high as 4.6 times was seen for **S-6** over **S-5** when using **A-25** as the annihilator (Fig. 9b). This work demonstrated for the first time the effectiveness of the supramolecular motif for enhancing TTA-UC without varying the inherent photophysical properties of sensitizers and annihilators.

Due to the equilibrium nature of supramolecular interactions, unbound sensitizers and annihilators may also contribute to upconversion (UC) emissions. Therefore, achieving a distinct “turn-

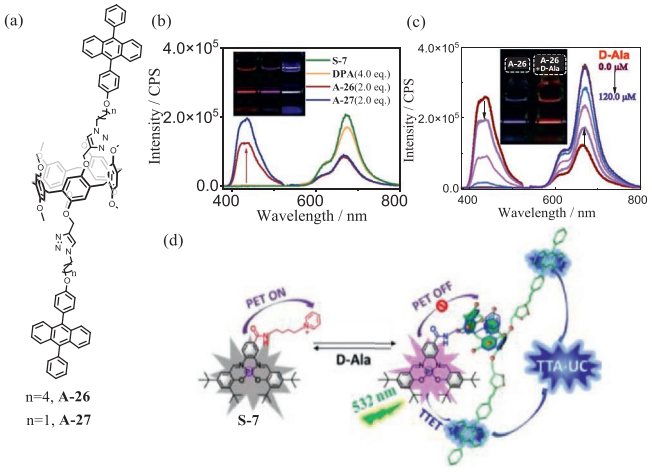



**Fig. 10.** (a) The chemical structures of annihilators **A-26** and **A-27**. (b) TTA-UC emission of DPA, **A-26**, and **A-27** sensitized by **S-7** in deaerated $CHCl_3$. Inset: Photographs of the emissions of the solution containing **S-7** and acceptors **DPA** (left), **A-26** (middle) or **A-27** (right). (c) UC emissions of **S-7**/**A-26** upon adding different concentrations of D-Ala (0.0–120.0 μmol/L) in deaerated $CHCl_3$. (d) A proposed mechanism of switching on TTA-UC by host-guest complexation. Reproduced with permission [14]. Copyright 2025, Elsevier.

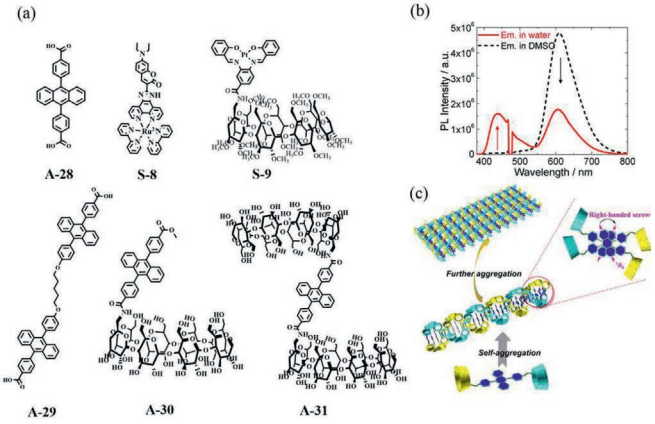



**Fig. 11.** (a) Chemical structures of annihilators **A-28**~**A-31**, sensitizer **S-8** and **S-9.** (b) The UC emission of **S-8** with **A-31** as the annihilator in water (red line) and in DMSO (black line). (c) schematic diagram of supramolecular self-assembled structures. Reproduced with permission [110]. Copyright 2018, Chemistry Europe.

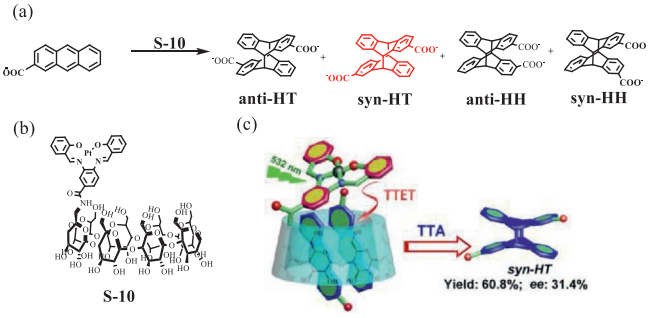



**Fig. 12.** (a) [4 + 4] Photocyclodimerization of **AC** Mediated by photosensitizers **S-10**. (b) Chemical structure of sensitizer **S-10**. (c) Schematic diagram of catalytic photochirogenesis. Reproduced with permission [24]. Copyright 2018, American Chemical Society.

on" effect in a supramolecular UC system remains challenging, yet it holds great promise for practical applications such as molecular sensing based on TTA-UC. To suppress UC emission originating from unbound components in such systems, a pyridinium cation was introduced into the Pt(II)–salophen complexes [14]. This modification induced photoinduced electron transfer (PET), effectively deactivating the excited state of the sensitizers and thereby quenching UC emission (Fig. 10d). However, when the pyridinium cation was encapsulated within the cavity of pillar[5]arene, PET was suppressed. Thus, by employing DPA-functionalized pillararene derivatives **A-26** and **A-27** as supramolecular annihilators (Fig. 10a), TTA-UC emission was significantly enhanced, the intensity was more than one hundred times greater than that of free DPA (Fig. 10b). An ON–OFF switching of UC emission was achieved through the addition of competitive guests (Fig. 10c), demonstrating the potential of these systems for molecular sensing and the construction of stimuli-responsive smart materials

Water-soluble supramolecular annihilators with DPA-attached-cyclodextrin derivatives were synthesized, the $\gamma$-cyclodextrin ($\gamma$-CD) unit serves as a molecular host for binding sensitizer, and the DPA moieties play a role as the annihilator. **A-30** and **A-31** (Fig. 11a) formed ribbon-like or helical nanoclusters in aqueous solutions *via* $\pi$–$\pi$ stacking aggregate and host–guest complexation (Fig. 11c), and the high fluorescent quantum yield of up to 82% (**A-30**) and 90% (**A-31**) was achieved, demonstrating that aggregation did not quench the fluorescence, which was highly beneficial for TTA-UC. A coordinated ruthenium complex (**S-8**) containing a coumarin unit serving as the guest of $\gamma$-CD was used as the sensitizer. Due to improved TTET process through host–guest complexation, and a facilitated TTA process along the orderly stacked annihilators through triplet-energy migration, a high TTA upconversion quantum yield of up to 6.9% was observed in pure water, which is significantly higher than the value (<0.5%) obtained in organic solvent of DMSO (Fig. 11b). The observed efficiency contrast stems primarily from molecular organization in aqueous media, within the nano-aggregates, the DPA annihilators adopt an ordered arrangement that creates efficient pathways for triplet exciton migration. This enables excitons generated on sensitizers to rapidly migrate and encounter annihilators, significantly boosting the overall TTA efficiency. In contrast, in DMSO, the bulky $\gamma$-CD grafted annihilator was molecularly dispersed, which severely impedes diffusion and annihilation and consequently limits the UC quantum yield [110].

Similarly, when the sensitizer was attached on a supramolecular hosts permethyl-$\beta$-cyclodextrin (PMCD), and DPA carboxylate (**A-28**) as well as its dimer (**A-29**) in which two DPA carboxylates were covalently linked with an alkyl chain, was served both as the guests of PMCD and annihilators, the TTET process was also greatly enhanced. Although both systems benefit from enhanced TTET *via* host-guest complexation, the dimer **A-29** exhibited much higher upconversion efficiency than the monomer **A-28**. This performance disparity can be attributed to the structural characteristics of **A-29**: Its extended hydrophobic framework possesses a stronger propensity for self-assembly in aqueous media, enabling the formation of more ordered supramolecular aggregates compared to **A-28**. Such ordered nanostructures provide the essential pathways for long-range triplet exciton migration, which is critical for achieving high-efficiency TTA in the diffusion-limited aqueous environment. These studies demonstrate that while host-guest complexation alone can optimize TTET, achieving efficient aqueous TTA-UC requires the further construction of ordered supramolecular architectures capable of supporting long-range exciton migration [111].

The accelerated TTET within host–guest complexes further enabled catalytic supramolecular photochirogenesis. In one representative system (Fig. 12), a schiff-base Pt(II) sensitizer (**S-10**) was grafted onto $\gamma$-cyclodextrin, while 2-anthracenecarboxylic acid (AC) served as both guest and annihilator. The $\gamma$-CD cavity of **S-10** created a chiral microenvironment which pre-organizing AC

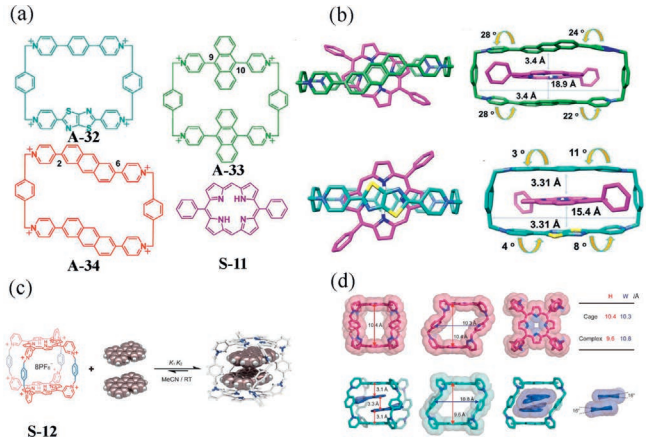



**Fig. 13.** (a) Chemical structures of annihilator **A-32**∼**A-34**. (b) Tubular representations of the solid-state superstructures of **A-34**⊃**S-11** (up) and **A-32**⊃**S-11** (down) obtained from single-crystal X-ray diffraction studies. Reproduced with permission [112]. Copyright 2020, American Chemical Society. (c) Schematic diagram of two perylene guest molecules in **S-12**. (d) Structures of the cage and complex obtained by X-ray crystallography. Reproduced with permission [113]. Copyright 2023, American Chemical Society.

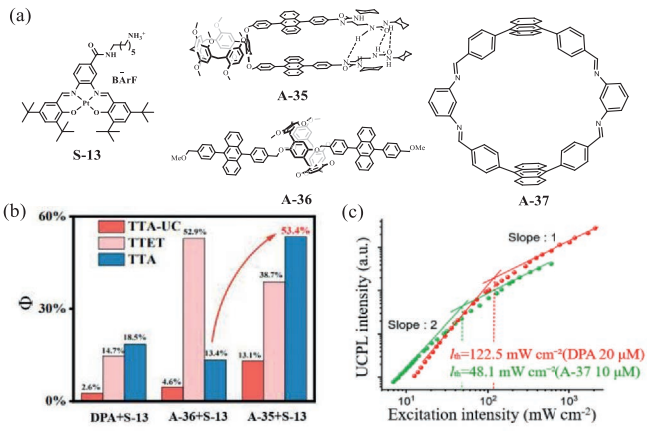



**Fig. 14.** (a) The chemical structures of the annihilator **A-35**∼**A-37**, and the sensitizers **S-13**. (b) Histogram of $\Phi_{UC}$, $\Phi_{TTET}$, and $\Phi_{TTA}$ of the UC systems with **S-13** as the sensitizer and **A-35**, **A-36** and DPA as the annihilator Reproduced with permission [15]. Copyright 2024, MDPI. (c) Excitation intensity dependence of UC emission intensity of **S-4**/DPA and **S-4**/**A-37** in deaerated chloroform. Reproduced with permission [115]. Copyright 2024, American Chemical Society.

molecules. Upon photoexcitation, triplet energy is transferred from **S-10** to the bound AC *via* TTET. Subsequent TTA generates a high-energy singlet anthracene intermediate, which then undergoes a stereocontrolled [4 + 4] photocycloaddition dimerization inside the chiral cavity (Fig. 12a). This confinement imparts significant enantioselectivity, favoring the formation of the *syn*-HT dimer with an enantiomeric excess (*ee*) of 31.4 %. Crucially, TTET from the host-bound sensitizer to the encapsulated AC proved far more efficient than to free AC in bulk solution (Fig. 12c). This allowed selective sensitization of the complexed AC, thereby enabling catalytic turnover. Consequently, a catalytic amount of **S-10** drove the photodimerization of AC, affording the *syn*-HT dimer in 31.4 % *ee* and 60.8 % relative yield [24].

Integrating TTA-UC functional components as structural units into macrocyclic frameworks enables the construction of well-defined, functionally integrated "molecular devices". Two primary design strategies exist: Incorporating the annihilator as part of the macrocyclic host or using sensitizers as building blocks to form molecular containers that encapsulate annihilators. In 2020, Stoddart *et al.* [112] designed box-like fluorescent tetracationic hosts (Fig. 13a) incorporating a thiazolothiazole or anthracene annihilators (**A-32**∼**A-34**). X-ray single-crystal diffraction showed that **A-32** has a cavity of 15.6 Å in length and 7.1 Å in width, which can fully accommodate a 5,15-diphenylporphyrin as a sensitizer. The $\pi$–$\pi$ stacking distance between host and guest was 3.31 Å, with significantly enhanced molecular planarity after complexation (Fig. 13b). Significantly, this host-guest complex showed a $\Phi_{UC}$ of 5.8 % in MeCN at a dilute concentration of **S-11** (20 μmol/L), the $\Phi_{UC}$ could be further optimized to 8.1 % by increasing **S-11** concentrations to 70 μmol/L. DFT calculations showed a series of close-energy excited states in **A-34**⊃**S-11** with a minimal singlet-triplet energy gap ($\Delta E_{ST}$) of 0.12 eV. Transient absorption studies showed several different triplet species with different lifetimes, indicating the population of the hybridized local and charge-transfer triplet state ($^3$HLCT). From these results, the authors draw a conclusion that the UC emission originates from the supramolecular host-guest complex instead of from the free UC components [112]. Similarly, a molecular container with two porphyrins (sensitizer) as the constitutional units was further synthesized (Fig. 13c). This container featured a well-defined cavity of approximately 9.6–10.4 Å in size (Fig. 13d) [113], and could successfully encapsulate two perylene molecules as annihilators. Moreover, it could host two annihilators with a suitable [$\pi$-$\pi$] distance of 3.2 – 3.5 Å (Fig. 13d). Therefore, when exciting the Q bands of the porphyrins with low-energy light, the upconverted fluorescence of the perylenes at 470 nm could be detected.

The spin statistical factor (*f*), which represents the probability of forming a bright singlet state from two annihilating triplet states, plays a critical role in determining the efficiency of triplet-triplet annihilation (TTA). Theoretical studies by Clark *et al.* suggested that a parallel alignment of chromophores leads to a higher *f* compared to a perpendicular arrangement [114]. To experimentally validate this hypothesis, two supramolecular annihilators, **A-35** and **A-36** were designed by functionalizing pillar[5]arene macrocycles with diphenylanthracene (DPA) units (Fig. 14a). In **A-36**, the two DPA units adopted a random orientation, whereas in **A-35**, intramolecular hydrogen bonding enforced a parallel configuration. This parallel alignment was shown to significantly enhance the TTA efficiency, increasing it from 13.4 % for **A-36** to 53.4 % for **A-35**. As a result, when sensitized by **S-13** (Fig. 14b), the upconversion quantum yield ($\Phi_{UC}$) of **A-35** reached 13.1 %, more than double that of the reference system **A-36** (4.6 %) [15].

In a related approach, Nobuhiro Yanai and colleagues [115] achieved a parallel orientation between two annihilator units by constructing a macrocyclic DPA dimer (Fig. 14a). Single-crystal X-ray diffraction analysis confirmed a fully parallel arrangement, with an interplanar angle of 0° between the anthracene planes. The presence of $\pi$–$\pi$ interactions was indicated by the short distance of 3.7 Å between adjacent aromatic rings. However, this close stacking resulted in a reduction of the fluorescence quantum yield from 98 % for monomeric DPA to 61.1 % for the macrocyclic system (**A-37**). Despite this quenching, the upconversion emission intensity of **A-37** remained comparable to that of DPA. Notably, under highly dilute conditions, **A-37** exhibited a substantially lower threshold intensity ($I_{th}$) than the DPA monomer (Fig. 14c), suggesting that intramolecular TTA between parallel-oriented chromophores can enhance TTA-UC performance. These findings collectively underscore the importance of chromophore orientation in the molecular design of high-efficiency annihilators.

## 3. Orderly arranging annihilators to achieve efficient TTA-UC in diffusion-limited systems

Although proof-of-principle demonstrations have validated that TTA-UC can enhance the performance of photovoltaic and pho-

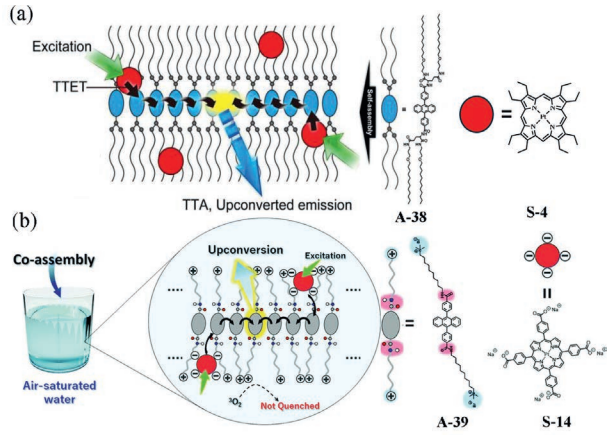



**Fig. 15.** (a) The chemical structure of Annihilator **A-38** and the photosensitizer **S-4**, and the schematic diagram of the self-assembly of this system. Reproduced with permission [119]. Copyright 2015, Springer Nature. (b) Annihilator **A-39** and the photosensitizer **S-14** and an illustration of the self-assembly of this upconversion system. Reproduced with permission [120]. Copyright 2016, Royal Society of Chemistry.

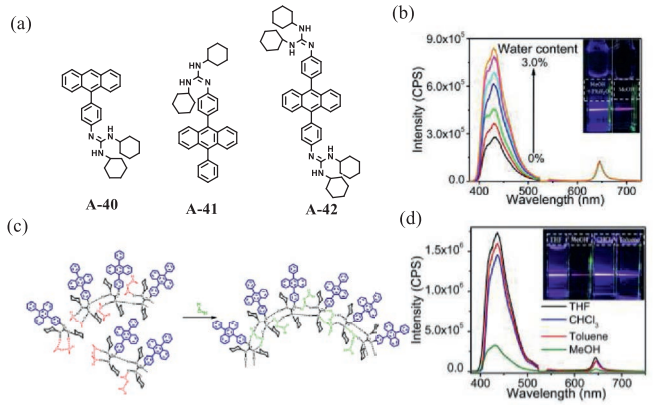



**Fig. 16.** (a) The chemical structures of Annihilator **A-40**∼**A-42**. (b) Emission spectra of the UC system **S-4/A-41** in deaerated MeOH with different content of water. Inset: Photographs of the emissions of the **S-4/A-41** UC systems in anhydrous MeOH and MeOH with 3% water. (c) Schematic diagram of aggregation morphology in methanol containing trace amounts of water (left). (d) Emission spectra of the **S-4/A-41** UC systems in different solvents. Insert: Photographs of the emissions of the **S-4/A-41** UC systems in different solvents Reproduced with permission [16]. Copyright 2023, Elsevier.

tochemical devices, its practical deployment remains limited by two major constraints: Low TTA-UC efficiency and the stringent requirement for deoxygenation to suppress triplet state quenching by molecular oxygen. To mitigate oxygen quenching, sensitizers and annihilators were embedded in solid polymer matrices or viscous liquid media. However, such confined environments significantly impede molecular diffusion, thereby reducing the efficiencies of TTA-UC and also much higher excitation power densities are often required, which limits the feasibility of these systems for real-world applications.

In response, a supramolecular strategy to orderly assembling the annihilator and sensitizers were proposed [116–118]. For instance, a novel amphiphilic annihilator (**A-38**) was designed, incorporating a solvophobic DPA core functionalized with multiple amide groups, coupled with solvophilic ether-linked alkyl chains *via* L-glutamate spacers [119]. The L-glutamate linker not only introduces molecular chirality but also facilitates the formation of hydrogen-bonding networks, thereby improving structural control and thermal stability. This amphiphilic structure promotes spontaneous self-assembly in organic media, resulting in well-defined nanotape-like monolayer assemblies with the annihilators orderly arranged which guaranteed fast triplet exciton migration (TEM) (Fig. 15a). By efficiently incorporate PtOEP (**S-4**) donor molecules in this supramolecular structure, highly efficient upconversion emission under both deaerated and aerated conditions was achieved with a $\Phi_{UC}$ record of 30% with a low threshold intensity ($I_{th}$) of 8.9 mW/cm$^2$. More importantly, due to the tightly packed, ordered assembly structure, oxygen permeation was signifcantly impeded, and therefore, TTA-UC emission remains largely stable in air-saturated environments, highlighting its potential for practical applications without stringent deoxygenation requirements.

Air-stable aqueous TEM-UC system was further developed. A cationic amphiphilic annihilator **A-39** was designed with quaternary ammonium groups positioned at both ends of the DPA chromophore [120]. A long alkyl chain functioned with amide groups was used to connect the DPA core and ammonium group to facilitate the formation of robust hydrogen bonds in an aqueous environment. **A-39** self-assembled into a highly ordered monolayer structure in water (Fig. 15b), when co-assemblied with an anionic sensitizer (**S-14**), efficient triplet energy transfer between the sensitizer and annihilator and fast TEM occurred, even in oxygen-saturated aqueous environments. This system stably achieved UC with a quantum efficiency of 7%.

By enabling TEM among aligned annihilators, triplet excitons can be efficiently transported without relying on molecular diffusion. This makes it possible to selectively accelerate the TTA step without interfering with TTET, thus constructing unique stimuli-responsive TTA-UC systems. In one representative study, three guanidyl-functionalized annihilators (**A-40**∼**A-42**) were synthesized (Fig. 16a). Among them, **A-41** self-assembled into highly ordered microparticles in aprotic solvents such as THF, chloroform, and toluene (Fig. 16c). The strong hydrogen bonding between guanidyl groups promoted a regular packing of DPA units, facilitating effective triplet exciton migration and resulting in a high $\Phi_{UC}$ of 10.2%. In contrast, the addition of methanol disrupted this ordered assembly, and thus significantly reduced the UC emissions (Fig. 16d), the $\Phi_{UC}$ was only 2.9%. Meanwhile, **A-40** and **A-42** exhibited only weak UC emission across all solvents tested, which was attributed to detrimental $\pi$–$\pi$ stacking of the anthracene cores. Notably, the hydrogen-bonded network of **A-41** could be restructured by introducing trace amounts of water (Fig. 16b). Upon adding 3% (v/v) water to methanol, the $\Phi_{UC}$ recovered from 2.9% to 9.2%. Importantly, since the TTET process remained unaffected, the residual phosphorescence of the sensitizer stayed unchanged and served as an internal reference. This enabled the development of a ratiometric sensor for trace water detection in methanol, achieving a detection limit as low as 0.084% (v/v) [16].

Gels have been widely utilized as matrices for TTA-UC. Their appeal lies not only in material-level advantages such as nonfluidity and good processability but also in their unique microscopic structure. The interconnected solution phase within gels allows for sufficient molecular diffusion of UC components, enabling TTA-UC performance comparable to that in liquid solutions [121–124]. Photon-upconverting hydrogels were fabricated through the co-assembly of gelatin, the nonionic surfactant Triton X-100 (TX100), and relevant upconversion chromophores [125]. Gelatin and TX100 formed a hierarchically organized matrix comprising hydrophobic microdomains capable of hosting high concentrations of chromophores (Fig. 17a). To enhance compatibility and dispersibility within this hydrogel network, the DPA annihilator was functionalized with a sulfonate group. This modification promoted molecular distribution and stability by interactions of polar sul-

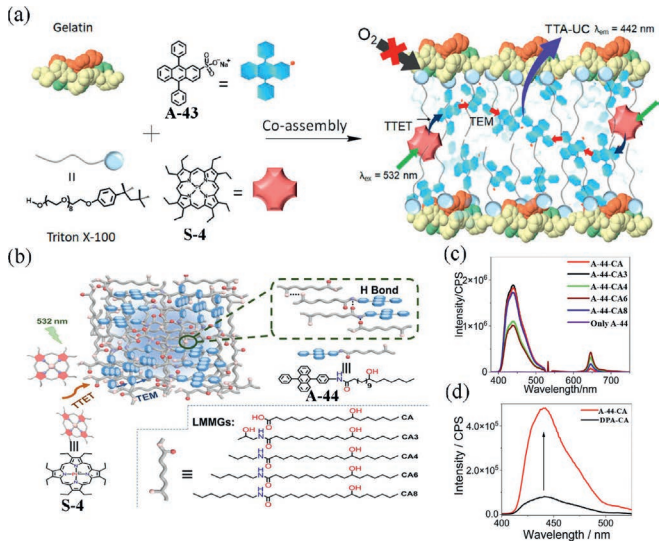



**Fig. 17.** (a) Schematic diagram of the G-TX & **A-43** & **S-4** copolymer aggregates in photonic upconversion hydrogel. Reproduced with permission [125]. Copyright 2018, American Chemical Society. (b) The structures of the LMMGs and annihilator **A-44** and the schematic diagram of orderly arranging **A-44** in the gel. (c) Emissions of above organogels under irradiation with a 532 nm laser. (d) UC emission intensity of the annihilators **A-44** and DPA sensitized by **S-4** in ***CA*** dried gels. Reproduced with permission [127]. Copyright 2025, Wiley.

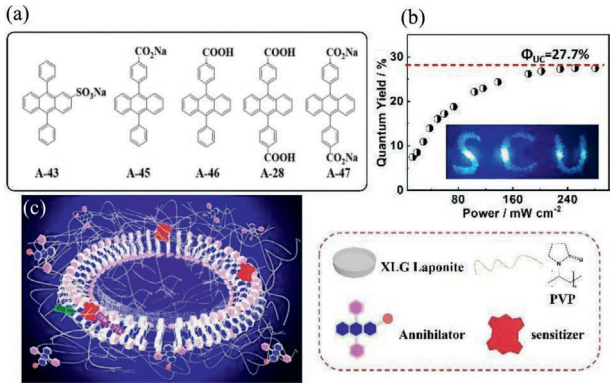



**Fig. 18.** (a) The chemical structures of annihilators **A-43**∼**A-47**. (b) UC quantum yields of the dry gel as a function of incident light power density; inset: UC emission spectra of 2.5 mmol/L **A-43** and 10 μmol/L **S-4** in the dry gel. (c) The diagram of the preparation of UC XLG/PVP hydrogel. Reproduced with permission [17]. Copyright 2022, Royal Society of Chemistry.

fonate moiety with the gelatin backbone and TX100. As a result, the system achieved TTA-UC with an efficiency of 13.5 %, a value comparable to the highest reported for aqueous UC systems. Notably, the dense hydrogen-bonding network inherent to the gelatin backbone acted as an effective oxygen barrier, significantly impeding $O_2$ diffusion into the hydrophobic chromophore-containing regions. This structural feature endows the hydrogel with exceptional air stability, enabling sustained UC emission under ambient atmospheric conditions without the need for deoxygenation.

Compared to hydrogels, organogels utilize an organic solvent as the dispersed phase, which is more favorable for TTA-UC. In 2015, Kimizuka and colleagues reported the preparation of supramolecular organogels through the self-assembly of a low-molecular-weight lipophilic gelator, *N*,*N*′-bis(octadecyl)-L-Boc-glutamic diamide (LBG), which formed nanofibrous networks capable of gelatinizing organic solvents [126]. The gelator contains multiple hydrogen-bonding groups, enabling long-range crystalline-like order within physically cross-linked nanofiber assemblies. Within these hydrogen-bond-stabilized nanofibers, both sensitizer and annihilator molecules were spontaneously concentrated, leading to an air-stable upconversion (UC) emission with a quantum yield of 3.5 % and a threshold intensity ($I_{th}$) of 1.5 mW/cm$^2$. Nevertheless, this system still relied on molecular diffusion within the internal solution phase to facilitate the TTA-UC process.

To eliminate the dependence on molecular diffusion and achieve efficient TTA-UC in solvent-free gel matrices, a subsequent study designed a series of low-molecular-mass gelators (LMMGs) derived from 12-hydroxystearic acid, along with a novel annihilator **A-44** (Fig. 17b), in which a 12-hydroxystearic acid unit was covalently linked to a DPA chromophore [127]. When co-assembled with the LMMGs, the DPA moiety of **A-44** became uniformly dispersed within the gel network. By chemically tailoring the LMMGs to optimize the organogel morphology, a high UC quantum yield of 13.4 % was attained (Fig. 17c). Remarkably, strong UC emission was maintained even after complete solvent removal from the organogels when **A-44** was employed as the annihilator. In contrast, systems using unmodified DPA showed a sixfold reduction in UC intensity under the same dry conditions (Fig. 17d).

The ordered arrangement of annihilators was further realized through an organic/inorganic hybridization strategy [17]. Laponite XLG, an inorganic nanomaterial with a diameter of around 25 nm and a thickness of 1–2 nm, was employed as the host matrix for upconversion components. This choice was motivated by the distinctive charge characteristics of laponite nanosheet, which possesses positively charged edges and negatively charged basal planes. A series of negatively charged annihilators (compounds **A-43**∼**A-47**) were synthesized and assembled in an orderly fashion along the nanodisc edges *via* electrostatic interactions (Fig. 18a). Polyvinylpyrrolidone (PVP) was incorporated into the upconversion system *via in-situ* radical polymerization of *N*-vinyl-2-pyrrolidone (NVP) (Fig. 18c). The introduction of PVP served a dual purpose: It promoted the monodispersion of the annihilator-loaded nanosheets and also functioned as an oxygen scavenger within the system. As a result, a remarkable upconversion quantum yield of 10 % was achieved in hydrogel under air. More importantly, even after complete solvent removal, the well-defined ordered structure was preserved, enabling efficient TTET and TTA. Under ambient conditions, the solid sample exhibited an upconversion quantum yield as high as 27.7 % (Fig. 18b), which represents the highest value reported to date for solid-state TTA-UC systems. This work demonstrates that by organically combining the templating effect of well-defined inorganic nanomaterials with the functional modification and integration capabilities of organic components, it is possible to construct advanced hybrid materials that simultaneously exhibit long-range order, excellent stability, and exceptional photon upconversion efficiency, marking a critical step toward the practical application of solid-state TTA-UC.

## 4. Conclusion and future outlook

This review summarizes recent advances in the design and assembly strategies of annihilators for efficient triplet–triplet annihilation upconversion (TTA-UC). Emerging annihilator systems include multichromophoric annihilators engineered for intramolecular TTA, supramolecular macrocycle-based assemblies that enhance both triplet–triplet energy transfer (TTET) and TTA processes, and annihilators with ordered molecular arrangements that facilitate efficient TTA-UC under diffusion-limited conditions. Strategies for the first two categories primarily aim to overcome diffusion-related limitations, whereas the third focuses on promoting rapid triplet exciton migration within organized molecular assemblies.

While multichromophoric annihilators designed for intramolecular TTA offer a promising approach, they do not consistently outperform single-chromophore systems relying on intermolecu-

lar TTA. Key molecular parameters such as planarity, geometry, and relative orientation significantly influence the efficiency of intramolecular TTA. In contrast, supramolecular macrocycle-based annihilators often co-assemble sensitizers and multiple annihilators in close proximity, thereby simultaneously enhancing TTET and TTA. This approach provides an effective means to improve TTA-UC performance without modifying the intrinsic photophysical properties of the individual components. Furthermore, achieving long-range ordered annihilator assemblies has emerged as a highly promising strategy for realizing efficient TTA-UC in solid state, as evidenced by an impressive upconversion quantum yield ($\Phi_{UC}$) of 23.6 % in a solvent-free solid system.

Despite these encouraging developments, challenges still exist, *e.g.* the structure–activity relationships in annihilator design are not yet fully elucidated, and strategies for the controlled assembling of both photosensitizers and annihilators into well-ordered architectures remain limited. Addressing these issues will require continued and focused efforts from the scientific community.

## CRediT authorship contribution statement

**Junjie Wen:** Writing – original draft, Formal analysis, Data curation. **Dantong Chen:** Methodology, Investigation, Formal analysis. **Hongli Cao:** Methodology, Formal analysis, Data curation. **Xue Li:** Methodology, Data curation. **Ying Qin:** Methodology, Data curation. **Cheng Yang:** Writing – review & editing, Supervision, Project administration, Funding acquisition. **Wanhua Wu:** Writing – review & editing, Supervision, Project administration, Funding acquisition, Formal analysis, Conceptualization.

## Declaration of competing interest

The authors declare that they have no known competing financial interests or personal relationships that could have appeared to influence the work reported in this paper.

## Acknowledgments

We acknowledge the support of this work by the National Natural Science Foundation of China (Nos. 22422108, 22171194, 22471182, 22271201, U25A20592), the Science & Technology Department of Sichuan Province (Nos. 2025JDRC0015, 2025ZNSFSC0125).

## References

[1] S. Izawa, M. Hiramoto, Nat. Photonics 15 (2021) 895–900.
[2] Y.J. Meng, D.X. Huang, H. Li, et al., Nat. Photonics 17 (2023) 73–81.
[3] B.D. Ravetz, A.B. Pun, E.M. Churchill, et al., Nature 565 (2019) 343–346.
[4] J. Zhou, Q. Liu, W. Feng, et al., Chem. Rev. 115 (2015) 395–465.
[5] L.L. Wei, C. Yang, W.H. Wu, Curr. Opin. Green. Sustain. Chem. 43 (2023) 100851.
[6] C.M. Cruz, I.R. Márquez, I.F.A. Mariz, et al., Chem. Sci. 9 (2018) 3917–3924.
[7] X.X. Zhu, H.X. Xu, Y.T. Liu, et al., Adv. Mater. 31 (2019) 1901240.
[8] X.K. Chen, X.D. Zhang, Y.L. Zhao, Chem. Soc. Rev. 54 (2025) 152–177.
[9] S.B. Liu, L. Yan, J.S. Huang, et al., Chem. Soc. Rev. 51 (2022) 1729–1765.
[10] Y.Y. Zhang, T.Y. Zhao, Y.M. Deng, et al., Nat. Commun. 16 (2025) 6080.
[11] V.I. Shlyapkina, M.N. Zharkov, D.E. Yakobson, et al., Biochem. Biophys. Res. Commun. 776 (2025) 152202.
[12] X.Y. Meng, Y. Xie, T. Shen, et al., Inorg. Chem. Commun. 167 (2024) 112672.
[13] B. Liu, Z.Y. Wang, Z.M. Liu, et al., J. Rare Earths 43 (2025) 909–921.
[14] C. He, R.L. Huang, L.L. Wei, et al., Chin. Chem. Lett. 36 (2025) 110103.
[15] Q.H. He, L.L. Wei, C. He, et al., Molecules 29 (2024) 2203.
[16] Y.J. Sun, L.L. Wei, S.J. Zhu, et al., Sens. Actuators B: Chem. 387 (2023) 133764.
[17] L.L. Wei, C.Y. Fan, M. Rao, et al., Mater. Horiz. 9 (2022) 3048–3056.
[18] S.J. Zhu, L.L. Wei, Y.J. Sun, et al., Adv. Opt. Mater. 11 (2023) 2300484.
[19] Z.G. Lin, P. Zhang, Y.Z. Yang, W.S. Liu, Chin. Chem. Lett. 36 (2025) 111194.
[20] V. Gray, D. Dzebo, M. Abrahamsson, et al., Phys. Chem. Chem. Phys. 16 (2014) 10345–10352.
[21] J. Pedrini, A. Monguzzi, F. Meinardi, Phys. Chem. Chem. Phys. 20 (2018) 9745–9750.
[22] Q.Y. Zhang, G.W. Luo, J.P. Chen, et al., Chin. Chem. Lett. 35 (2024) 109009.
[23] A. Grippa, N. Rebrova, P. Zdeb-Stańczykowska, P.J. Dereń, J. Lumin. 288 (2025) 121541.
[24] M. Rao, K. Kanagaraj, C.Y. Fan, et al., Org. Lett. 20 (2018) 1680–1683.
[25] S.S. Liu, H.Y. Liu, Y.J. Hu, et al., Chem. Eng. J. 452 (2023) 139203.
[26] Y.C. Chou, C.L. Li, J.C. Lin, et al., Ceram. Int. 51 (2025) 53812–53821.
[27] Y. Chen, L. Li, G.H. Han, et al., Chin. Chem. Lett. 36 (2025) 110458.
[28] P.F. Peng, N. Wu, L.X. Ye, et al., ACS Nano 14 (2020) 16672–16680.
[29] D.J. Lu, F. Fang, D.D. Jia, et al., J. Lumin. 286 (2025) 121421.
[30] C. Liu, T. Wu, L.J. Deng, et al., Chin. Chem. Lett. 35 (2024) 109307.
[31] N.T. Nguyen, J. Kim, X.T. Le, et al., ACS Nano 17 (2023) 382–401.
[32] V.K. Thammannagowda, K.G.G. Shivanna, S. Panier, P. Kalappa, Next Mater. 9 (2025) 101314.
[33] S.K. Y.Cakmak, S. Duman, et al., Angew. Chem. Int. Ed. 50 (2011) 11937–11941.
[34] X.M. Chen, M. Lyu, J.L. Liu, et al., Cell Biomater. (2025) 100247.
[35] Z. Luan, X.L. Ma, Q.X. Zhao, et al., Chem. Eng. J. 488 (2024) 150611.
[36] Y.Q. Liu, S.L. Zhang, K. Jiang, et al., Chin. Chem. Lett. 36 (2025) 110282.
[37] W.B. Zhou, Y.F. Gao, X.Y. Feng, et al., Chin. Chem. Lett. 36 (2025) 109763.
[38] W.H. Wu, X.N. Cui, J.Z. Zhao, Chem. Commun. 49 (2013) 9009–9011.
[39] W.H. Wu, J.Z. Zhao, J.F. Sun, et al., J. Mater. Chem. C 1 (2013) 705–716.
[40] Z.J. Wang, M.Y. Wu, X. Cui, et al., ACS Nano 19 (2025) 25596–25616.
[41] J. Wellauer, B. Pfund, I. Becker, et al., J. Am. Chem. Soc. 147 (2025) 8760–8768.
[42] M.Y. Zhang, H.J. Feng, J.Y. Li, et al., Adv. Mater. 37 (2025) 2502150.
[43] C.Y. Fan, L.L. Wei, T. Niu, et al., J. Am. Chem. Soc. 141 (2019) 15070–15077.
[44] D. Yang, P.F. Duan, M.H. Liu, Angew. Chem. Int. Ed. 57 (2018) 9357–9361.
[45] P. Vázquez-Domínguez, O. Journaud, N. Vanthuyne, et al., Dalton. Trans. 50 (2021) 13220–13226.
[46] J.P. Wei, J.C. Li, D. Sun, et al., Adv. Funct. Mater. 28 (2018) 1706310.
[47] D. Yang, J.L. Han, M.H. Liu, P.F. Duan, Adv. Mater. 31 (2019) 1805683.
[48] D. Kim, D.R. Whang, S.Y. Park, J. Am. Chem. Soc. 138 (2016) 8698–8701.
[49] L.K. McKenzie, H.E. Bryant, J.A. Weinstein, Coord. Chem. Rev. 379 (2019) 2–29.
[50] F. Doettinger, Y. Yang, M. Karnahl, S. Tschierlei, Inorg. Chem. 62 (2023) 8166–8178.
[51] J. Steube, A. Kruse, O.S. Bokareva, et al., Nat. Chem. 15 (2023) 468–474.
[52] O.S. Wenger, J. Am. Chem. Soc. 140 (2018) 13522–13533.
[53] F. Doettinger, J. Sagaya, G. Morselli, O.S. Wenger, J. Am. Chem. Soc. 147 (2025) 43013–43028.
[54] S.S. Yan, G.Y. Xing, X.Y. Yuan, et al., J. Colloid. Interface Sci. 677 (2025) 666–674.
[55] P. Dash, S. Thirumurugan, Y.L. Chen, et al., Int. J. Pharm. 675 (2025) 125545.
[56] C.Y. Fan, X.F. Wei, W.H. Wu, C. Yang, Org. Lett. 26 (2024) 950–954.
[57] L.M. Li, S. Kamal, A.M. Polgar, Z.M. Hudson, J. Phys. Chem. B 128 (2024) 8997–9004.
[58] Y.X. Wei, K.B. An, X.S. Xu, et al., Adv. Opt. Mater. 12 (2024) 2301134.
[59] Y.L. Liu, H.Y. Wang, F.F. Ke, et al., Adv. Ther. 7 (2024) 2300400.
[60] Y.L. Zhao, Y.N. Wu, W.L. Chen, et al., Adv. Opt. Mater. 10 (2022) 2102275.
[61] V. Gray, P. Xia, Z.Y. Huang, et al., Chem. Sci. 8 (2017) 5488–5496.
[62] S. He, N.J.J. Johnson, V.A.N. Huu, et al., Chem. Mater. 30 (2018) 3991–4000.
[63] H. Ge, D.Y. Wang, Y. Pan, et al., Angew. Chem. Int. Ed. 59 (2020) 8133–8137.
[64] Q. Yang, C. Zhao, J. Zhao, Y. Ye, Opt. Mater. Express. 7 (2017) 913–923.
[65] R.J. Zuo, Z.C. Ye, H. Liang, et al., Photochem. Photobiol. Sci. 23 (2024) 1309–1321.
[66] K. Okumura, K. Mase, N. Yanai, N. Kimizuka, Chem. Eur. J. 22 (2016) 7721–7726.
[67] R.S. Khnayzer, J. Blumhoff, J.A. Harrington, et al., Chem. Commun. 48 (2012) 209–211.
[68] S. Amemori, Y. Sasaki, N. Yanai, N. Kimizuka, J. Am. Chem. Soc. 138 (2016) 8702–8705.
[69] N. Nishimura, J.R. Allardice, J. Xiao, et al., Chem. Sci. 10 (2019) 4750–4760.
[70] O.S. Kwon, H.S. Song, J. Conde, et al., ACS Nano 10 (2016) 1512–1521.
[71] B. Joarder, A. Mallick, Y. Sasaki, et al., ChemNanoMat 6 (2020) 916–919.
[72] J.H. Kim, F. Deng, F.N. Castellano, J.H. Kim, Chem. Mater. 24 (2012) 2250–2252.
[73] L.L. Wei, C. Yang, W.H. Wu, Mater. Chem. Front. 7 (2023) 3194–3208.
[74] T. Ogawa, M. Hosoyamada, B. Yurash, et al., J. Am. Chem. Soc. 140 (2018) 8788–8796.
[75] F. Marsico, A. Turshatov, R. Peköz, et al., J. Am. Chem. Soc. 136 (2014) 11057–11064.
[76] M.F. Wu, D.N. Congreve, M.W.B. Wilson, et al., Nat. Photonics 10 (2016) 31–34.
[77] T. Morifuji, Y. Takekuma, M. Nagata, ACS Omega 4 (2019) 11271–11275.
[78] F. Saenz, A. Ronchi, M. Mauri, et al., Adv. Funct. Mater. 31 (2021) 2004495.
[79] Y.X. Wei, Y. Wang, Q.H. Zhou, et al., Phys. Chem. Chem. Phys. 22 (2020) 26372–26382.
[80] A. Banerjee, K. De, U. Bhattacharjee, J. Phys. Chem. B 128 (2024) 849–856.
[81] C. Wang, F. Reichenauer, W.R. Kitzmann, et al., Angew. Chem. Int. Ed. 61 (2022) e202202238.
[82] Z.A. VanOrman, A.S. Bieber, S. Wieghold, L. Nienhaus, Chem. Mater. 32 (2020) 4734–4742.
[83] A. Olesund, V. Gray, J. Mårtensson, B. Albinsson, J. Am. Chem. Soc. 143 (2021) 5745–5754.
[84] C. Schad, E. Avellanal-Zaballa, E. Rebollar, et al., Phys. Chem. Chem. Phys. 24 (2022) 27441–27448.
[85] A. Haraguchi, K. Goushi, S. Sasaki, C. Adach, J. Phys. Chem. Lett. 16 (2025) 5173–5179.
[86] D. Dzebo, K. Börjesson, V. Gray, et al., J. Phys. Chem. C 120 (2016) 23397–23406.
[87] F. Edhborg, H. Bildirir, P. Bharmoria, et al., J. Phys. Chem. B 125 (2021) 6255–6263.

[88] K. Higashi, T. Okamoto, N. Iwaya, et al., Angew. Chem. Int. Ed. 64 (2025) e202503846.
[89] C.W. Lin, W.T. Chiang, M.M. Lee, et al., J. Chin. Chem. Soc. 72 (2025) 1183–1197.
[90] S.H. Lee, M.A. Ayer, R. Vadrucci, et al., Polym. Chem. 5 (2014) 6898–6904.
[91] A.J. Tilley, B.E. Robotham, R.P. Steer, K.P. Ghiggino, Chem. Phys. Lett. 618 (2015) 198–202.
[92] A.J. Tilley, M.J. Kim, M. Chen, K.P. Ghiggino, Polymers 54 (2013) 2865–2872.
[93] P.C. Boutin, K.P. Ghiggino, T.L. Kelly, R.P. Steer, J. Phys. Chem. Lett. 4 (2013) 4113–4118.
[94] A.B. Pun, S.N. Sanders, M.Y. Sfeir, et al., Chem. Sci. 10 (2019) 3969–3975.
[95] C. Gao, S.K.K. Prasad, B. Zhang, et al., J. Phys. Chem. C 123 (2019) 20181–20187.
[96] M. Kanoh, Y. Matsui, K. Honda, et al., J. Phys. Chem. B 125 (2021) 4831–4837.
[97] W.J. Sun, A. Ronchi, T.H. Zhao, et al., J. Mater. Chem. C 9 (2021) 14201–14208.
[98] J.L. Han, P.F. Duan, X.G. Li, M.H. Liu, J. Am. Chem. Soc. 139 (2017) 9783–9786.
[99] A. Ronchi, P. Brazzo, M. Sassi, et al., Phys. Chem. Chem. Phys. 21 (2019) 12353–12359.
[100] S. Mattiello, S. Mecca, A. Ronchi, et al., ACS Energy Lett. 7 (2022) 2435–2442.
[101] X.N. Cui, J.Z. Zhao, Z. Mohmood, C.S. Zhang, Chem. Rec. 16 (2016) 173–188.
[102] A. Monguzzi, R. Tubino, F. Meinardi, Phys. Rev. B 77 (2008) 155122.
[103] S. Jin, K. Sugawa, N. Takeshima, et al., ACS Photonics 5 (2018) 5025–5037.
[104] X.K. Yu, F.R. Gao, W.Y. Zhao, et al., Dalton. Trans. 51 (2022) 9314–9322.
[105] T.J.B. Zähringer, J.A. Moghtader, M.S. Bertrams, et al., Angew. Chem. Int. Ed. 62 (2023) e202215340.
[106] K.J. Xu, J.Z. Zhao, X.N. Cui, J. Ma, J. Phys. Chem. A 119 (2015) 468–481.
[107] H.Q. Zhou, J.X. Lin, S.G. Wan, W. Lu, Phys. Chem. Chem. Phys. 24 (2022) 29151–29158.
[108] H. Liang, X.Y. Liu, L.T. Tang, et al., Chin. Chem. Lett. 34 (2023) 107515.
[109] C.Y. Fan, W.H. Wu, J.J. Chruma, et al., J. Am. Chem. Soc. 138 (2016) 15405–15412.
[110] W. Xu, W.T. Liang, W.H. Wu, et al., Chem. Eur. J. 24 (2018) 16677–16685.
[111] H.X. Lai, T. Zhao, Y.R. Deng, et al., Chin. Chem. Lett. 30 (2019) 1979–1983.
[112] I. Roy, A. Garci, Y. Beldjoudi, et al., J. Am. Chem. Soc. 142 (2020) 16600–16609.
[113] H.L. Chen, I. Roy, M.S. Myong, et al., J. Am. Chem. Soc. 145 (2023) 10061–10070.
[114] D.G. Bossanyi, Y. Sasaki, S.Q. Wang, et al., JACS Au 1 (2021) 2188–2201.
[115] C.H. Mulyadi, M. Uji, B. Parmar, et al., Precis. Chem. 2 (2024) 539–544.
[116] W. Ahmad, J.J. Wang, H.H. Li, et al., Coord. Chem. Rev. 439 (2021) 213944.
[117] V. Gray, K. Moth-Poulsen, B. Albinsson, M. Abrahamsson, Coord. Chem. Rev. 362 (2018) 54–71.
[118] P.F. Duan, N. Yanai, N. Kimizuka, J. Am. Chem. Soc. 135 (2013) 19056–19059.
[119] T. Ogawa, N. Yanai, A. Monguzzi, N. Kimizuka, Sci. Rep. 5 (2015) 10882.
[120] H. Kouno, T. Ogawa, S. Amemori, et al., Chem. Sci. 7 (2016) 5224–5229.
[121] M.A. Kuzina, D.D. Kartsev, A.V. Stratonovich, P.A. Levkin, Adv. Funct. Mater. 33 (2023) 2301421.
[122] K. Sripathy, R.W. MacQueen, J.R. Peterson, et al., J. Mater. Chem. C 3 (2015) 616–622.
[123] P.F. Duan, D. Asthana, T. Nakashima, et al., Faraday Discuss. 196 (2017) 305–316.
[124] R. Vadrucci, C. Weder, Y.C. Simon, Mater. Horiz. 2 (2015) 120–124.
[125] P. Bharmoria, S. Hisamitsu, H. Nagatomi, et al., J. Am. Chem. Soc. 140 (2018) 10848–10855.
[126] P.F. Duan, N. Yanai, H. Nagatomi, N. Kimizuka, J. Am. Chem. Soc. 137 (2015) 1887–1894.
[127] J. Chen, P.Y. Wang, J.B. Liu, C. Yang, W.u W, Chin. J. Chem. 43 (2025) 2021–2028.